Advanced Steel Construction – Vol. 22 No. 1 (2026) 37–47
DOI:10.18057/IJASC.2026.22.1.4

EXPERIMENTAL STUDY ON STATIC PERFORMANCE OF SINGLE-LAYER SADDLE-SHAPED CABLE NET STRUSTURES

Jie Qin [1, 3], Hao Zhang [2], Guo-Jun Sun [2, *], Yu Xue [2], De-Qing You [4] and Jin-Zhi Wu [2]

[1] *University of Emergency Management, Langfang 065201, China*
[2] *Beijing University of Technology, Beijing 100124, China*
[3] *Hebei Key Laboratory of Civil Engineering Catastrophe Control and Disaster Emergency Response, Langfang 065201, China*
[4] *Beijing Building Construction Research Institute Co., Ltd., Beijing, 100039, China*
** (Corresponding author: E-mail: sunguojun@bjut.edu.cn)*

ABSTRACT

This study investigates the single-layer cable-net roof structure of the Xiatian Cultural Park Stadium by conducting a 1:10 scale model experiment to systematically examine the internal forces and deformations under various static loading conditions. The experiment incorporates full-span loading scenarios, and in conjunction with finite element simulations, analyzes and compares the force and deformation responses of the load-bearing cables, ring cables, diagonal cables, anti-wind cables, and back cables. The results demonstrate that, during loading, the cable forces and node displacements in all groups exhibit a linear relationship with the applied load. Among these, the ring cables sustain the highest internal forces, indicating their role as the primary load-bearing elements of the structure. Moreover, the finite element analysis results for static performance show close agreement with the experimental data, with discrepancies remaining within an acceptable range. This consistency verifies the accuracy of the numerical simulation method and confirms the reliability of the experimental results. The findings offer valuable reference data for the structural design and optimization of similar systems.

ARTICLE HISTORY

Received: 3 March 2025
Revised: 8 July 2025
Accepted: 18 July 2025

KEYWORDS

Single-layer cable structure;
Cable net structure;
Scaled model experiment;
Static loading test;
Mechanical performance

1. Introduction

Cable-net structures represent a significant form of tensile architecture, characterized by efficient stress distribution, diverse geometric configurations, effective force transmission, and substantial reductions in steel consumption. These advantages also contribute to the realization of sustainable building objectives, making cable-net systems a widely adopted structural solution in contemporary architecture [1]. Such structures are extensively used in large-span spatial applications. Single-layer cable-net systems typically consist of two sets of cables with opposing curvatures: the downward-curved load-bearing cables primarily support the dead and live loads of the roof, while the upward-curved tension cables function as stabilizing elements, resisting uplift forces induced by wind loads [2]. The elliptical boundary, saddle-shaped single-layer cable-net structure is notable for its elegant form and has seen application both domestically and internationally—for example, in the London Velodrome, Suzhou Olympic Sports Center Swimming Hall, and the National Speed Skating Oval. In recent years, it has undergone rapid development and broader implementation in China [3][4].

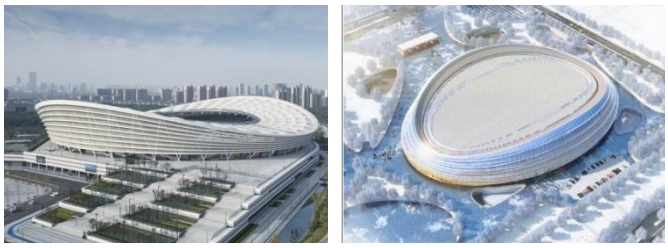

(a) Suzhou Olympic Sports Center Gymnasium (b) National Speed Skating Oval

Fig. 1 Typical saddle-shaped cable network construction

Current research on reticulated structures, both domestically and internationally, primarily focuses on aspects such as shape finding, construction methods, and mechanical performance. Schek [5] introduced the force-density method to perform preliminary shape finding for cable-net structures. Li et al. [6] employed a modified force-density method to analyze the shape finding of saddle-shaped orthotropic cable networks, applying this method to systems without an inner ring cable and achieving results closely aligned with numerical solutions. Li et al. [7] further proposed an innovative minimum surface finding method for cable-net structures, which significantly improved the iteration speed of the shape-finding process.Cable structures exhibit pronounced nonlinear behavior, distinguishing them from rigid structures. Unlike rigid systems, the performance of cable structures in meeting design requirements is closely tied to their construction processes [8]. A review of engineering cases, both in China and abroad, indicates that construction methods for saddle-shaped cable-net structures can be broadly categorized into three main types. The first method involves the use of auxiliary scaffolding, as seen in the construction of Calgary Stadium in Canada [9]. The cable system is laid atop the scaffolding and then tensioned to complete the cable-net installation. The second method entails overall lifting of the cable net, similar to the construction approach used for radial cable-net structures, exemplified by the Olympic Sports Center in Munich, Germany [10]. The third method is high-altitude assembly, in which stabilizing cables are delivered from outside the construction site to designated elevated positions using a cable-lowering technique. This method was applied in the construction of the cable-net roof at the Suzhou Swimming Pool [11]. Currently, engineers in China predominantly adopt the second method, involving the overall lifting of the cable net followed by sequential tensioning and batch installation. In the absence of established precedents, Gao et al. [12] proposed a construction method consisting of the overall lifting of the load-bearing cables, followed by unified tensioning of the stabilizing cables. This approach incorporates auxiliary measures such as accounting for passive forces in curtain wall cables and releasing the horizontal constraints of the outer ring beam supports. Final calculations confirmed that the shaping effect achieved was ideal. In addition to overall lifting, a few projects have employed high-altitude scaffolding. For example, the double-layer cable net of the Yangzhou Sports Park Swimming and Diving Hall was assembled midair using this method. Installation followed the principle of primarily tensioning the lower cables, with the upper cables serving as secondary supports.

Regarding the construction of cable-net structures, the methods vary depending on factors such as the construction site, hardware facilities, and economic conditions[13]. Consequently, their applicable scopes differ. Regardless of the method employed, it is essential to ensure that the structure remains in a low-stress state for as long as possible, while the duration in a high-stress state should be minimized during the construction process[14][15].The study of the static performance of cable nets primarily focuses on the shape and force changes of the cable net under static loads such as self-weight and snow load. The research on the dynamic performance of cable nets mainly investigates the structural natural frequencies and the response of the structure under dynamic loading. Although the negative curvature and relatively high prestress level make the cable net inherently "stiff," it still exhibits strong nonlinear behavior under load [16]. The stiffness of the structure itself is related to factors such as the deflection of the cable net, the magnitude and distribution of prestress, and the structural span-to-rise ratio. Generally, the control variable

method can be used to determine the extent of the influence of these factors on the cable net. Lu [17], based on a hub-and-spoke type single and double-layer hybrid cable net structure, found that the influence of wind suction on the internal forces and vertical displacement of the structure is greater than that of live loads, while the effect of temperature variations is negligible. Fabio et al. [18] conducted a full-scale static experiment on a single-layer cable net and investigated the effects of three different types of failure on the static performance of the cable net. The experimental results indicated that the failure of the connections between the cables had minimal impact on the static performance of the structure. In contrast, failure at the anchorage points of the cables significantly affected the structure. Furthermore, the damage itself had a greater influence on node displacements than on internal forces. Sun et al. [19] studied the inflection point behavior of a complex single-layer cable net model under horizontal loading, taking into account the effects of different prestress levels and glass stiffness.

This study focuses on the roof structure of the Xiatian Cultural Park Stadium. A 1:10 scaled model of the single-layer, saddle-shaped cable-net structure was designed and constructed for static loading experiments. The effects of different loading levels and load types on cable forces and displacements were examined under three static loading conditions. Based on the experimental findings, a corresponding finite element model was developed using ANSYS software at the same scale. The simulation results were then compared with the experimental data to validate the model, providing practical guidance for the structural design and application of cable-net systems in engineering practice.

2. Introduction of the test model

2.1. Engineering background

As shown in Fig. 2, the subject of this study is the roof structure of the Xiatian Cultural Park Stadium. The roof adopts a single-layer reticulated shell system with one rigid boundary and three flexible boundaries. The span of the structure measures 210 m × 54 m. The overall system comprises crescent-shaped steel ring beams and steel inclined columns serving as boundary conditions. The downward-curved load-bearing cables and upward-curved stabilizing cables are arranged orthogonally to form the single-layer reticulated shell. The structure is connected to the masts through ring cables and boundary cables, while backstay cables are employed for balance. This project introduces an innovative design that builds upon the conventional single-layer reticulated shell system, featuring one rigid boundary and three open, flexible line boundaries. The flexible boundaries are realized through the use of masts and backstay cables, enabling the structure to achieve large spans and wide open spaces. The overall structural form is novel, with a roof that appears light and elegant yet structurally robust. This configuration represents a new type of structural system that has not previously been seen in either domestic or international applications.

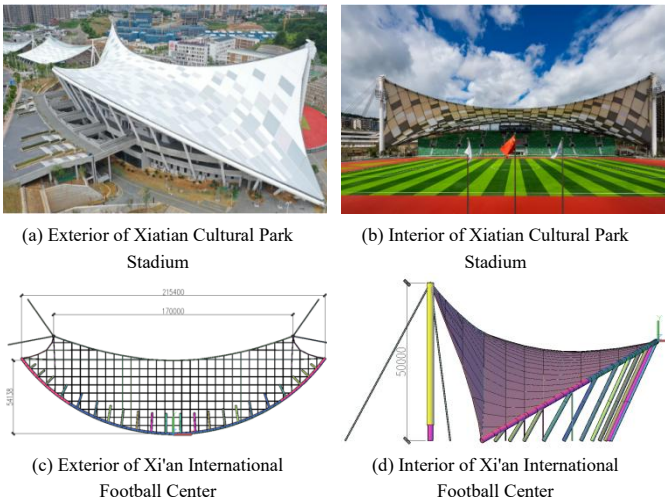

(a) Exterior of Xiatian Cultural Park Stadium

(b) Interior of Xiatian Cultural Park Stadium

(c) Exterior of Xi'an International Football Center

(d) Interior of Xi'an International Football Center

Fig. 2 Roof of Xiatian Cultural Park Stadium

2.2. Similitude law

Due to the large dimensions of the original structure and considering factors such as the testing site limitations, the model design was based on similarity theory, with a geometric scaling ratio of 1:10. The ratios of other physical quantities between the scaled model and the original structure were determined using magnitude analysis [20][21], as shown in Table 1.

Table 1
Similarity ratio between test model and actual structure

Physical property	Physical parameter	Symbol	Similarity ratio
Material Property	Elastic Modulus	S_E	1:1
	Stress	S_σ	1:1
	Poisson's Ratio	S_μ	1:1
	Density	S_ρ	1:1
Geometric Property	Span	S_L	1:10
	Area	S_A	1:100
	Strain	S_ε	1:1
Load Property	Concentration force	S_P	1:100

2.3. Model size and component specifications

As shown in Fig 3, the model is composed of supporting steel structure and single-layer cable net structure. The steel structure members include steel ring beam, steel inclined column, steel mast, steel mast support. The scale is designed according to the geometric scale of 1:10, and the similarity ratio of EA is 1:100. According to the actual materials that can be purchased, the final scale design is similar, such as the following Table 2, which basically meets the similarity ratio requirements. The steel ring beam, steel inclined column, steel mast and its support adopt welded steel pipe, and the material used is Q355B. The steel inclined column support adopts square tube, 150*150*5, and the steel grade is Q235B.

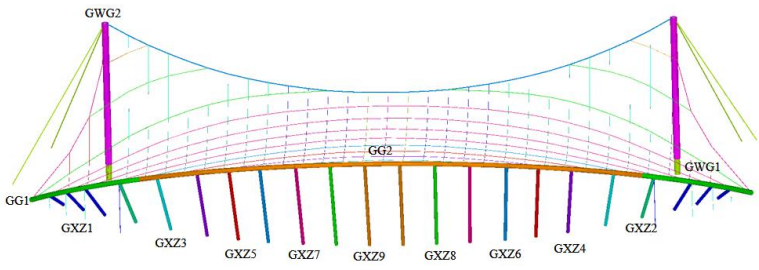

Fig. 3 Schematic diagram of steel members numbering

Table 2
Specifications and dimensions of beam

		Original model			Scale model			
Member type	Section type	Diameter/ mm	Thickness/ mm	Cross-sectional area/ mm²	Diameter/ mm	Thickness/ mm	Cross-sectional area/ mm²	EA similar ratio
GG1	Circular tube	1500	50	227766	152	5.75	2642	1:86
GG2		1500	40	183469	152	3.75	1746	1:105
GWG		2000	80	482534	203	7.75	4754	1:102
GXZ1		1000	30	91420	102	7.75	1157	1:79
GXZ2		1000	70	204518	102	7.75	2295	1:89
GXZ3		1000	80	231221	102	7.75	2295	1:101
GXZ4		1000	60	177186	102	5.75	1739	1:102
GXZ5		1000	40	120637	102	3.75	1157	1:104
GXZ6		1000	60	177186	102	5.75	1739	1:102
GXZ7		1000	65	190930	102	7.75	2295	1:83
GXZ8		1000	60	177186	102	5.75	1739	1:102
GXZ9		1000	50	149226	102	5.75	1739	1:86

As the Fig 4 shown, the single-layer cable network primarily comprises three main components: load-bearing cables(CS), anti-wind cables(KS), diagonal cable(XS), ring cables(HS) and back cables(BS). The EA similarity ratio is 1:100 for the design of drawbars according to the principle of stress similarity, and the following table shows the results of the design of drawbars. As for the material, the actual engineering ropes are all sealed cables, and the model test uses sealed cables and steel cables. the EA similarity ratio is about 1:100, which basically meets the requirements.

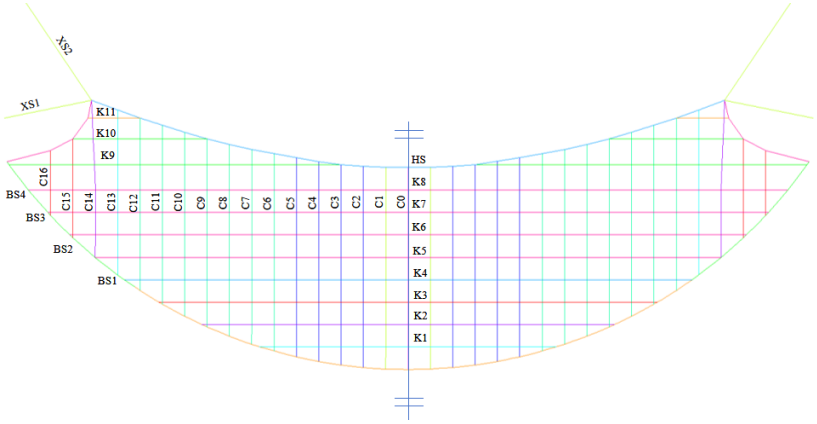

Fig. 4 Schematic diagram of cables numbering

Table 3
Specifications and dimensions of cables

Cables	Original model			Scale model			
	Specifications	Breaking force/kN	E/Mpa	Specifications	Breaking force/kN	E/Mpa	EA similar ratio
Load-bearing cables	Φ40	1580	1.6×10^5	Φ7	49.5	1.5×10^5	1:41
	Φ50	2470	1.6×10^5	Φ7	49.5	1.5×10^5	1:64
	Φ50	2470	1.6×10^5	Φ7	49.5	1.5×10^5	1:64
	Φ55	2170	1.6×10^5	Φ7	49.5	1.5×10^5	1:80
Anti-wind cables	Φ75	5620	1.6×10^5	Φ10	93.8	1.5×10^5	1:73
	Φ80	6390	1.6×10^5	Φ14	184.0	1.5×10^5	1:83
	Φ95	9110	1.6×10^5	Φ14	184.0	1.5×10^5	1:116
Ring cables Side-ring cables	Φ90	8090	1.6×10^5	Φ14	184.0	1.5×10^5	1:104
	Φ90	8090	1.6×10^5	Φ14	184.0	1.5×10^5	1:104
Back cables	Φ95	9110	1.6×10^5	Φ14	184.0	1.5×10^5	1:116
	Φ105	11100	1.6×10^5	Φ20	363.0	1.5×10^5	1:71
Diagonal cables	Φ125	15800	1.6×10^5	Φ26	660.0	1.5×10^5	1:103

3. Test scheme

3.1. Test load conditions

According to the design basis related to the single-layer saddle-shaped cable network structure of the stadium of Xiatian Cultural Park, the dead load, which includes the membrane structure, sound insulation, sunshade ceiling, and other hanging components, is 0.2 kN/m² . The live load is 0.3 kN/m² , the wind

load reference design institute MIDAS model export results, as specified in the Load Code for Building Structures (GB50009-2012) [22]. The load combinations are shown in Table 4. The distribution of load points is shown in Fig. 5.Although only 22 loading points were available, their layout was carefully optimized using a grid-based scheme to achieve a relatively uniform load distribution.

Table 4
Test conditions

Loading cases	Load distributions	Load composition
I	Full-span distribution	1.3×D+1.5×L
II	Full-span distribution	1.3×D+1.5×WP
III	Full-span distribution	1.3×D+1.5×WS

Note:D, L, WP, WS represent dead load, live load, wind pressure load and wind suction load respectively.

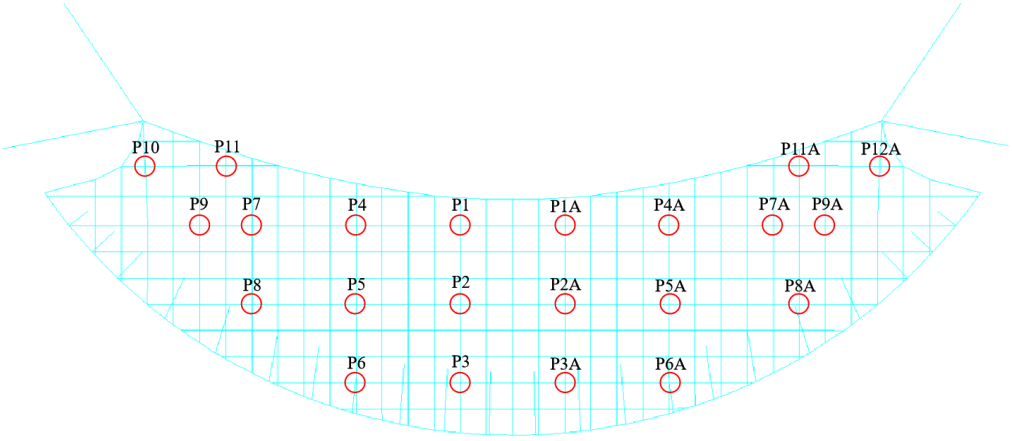

Fig. 5 Schematic diagram of loading points distribution

3.2. Loading method and load point location

During the static loading tests, the applied load required multiple adjustments to achieve the desired experimental conditions. Hence, the electro-servo loading control system was employed to perform the loading process. As shown in theFig 6, this system driven by an electric motor and integrated with servo control technology, enables precise control of load, velocity, and displacement.

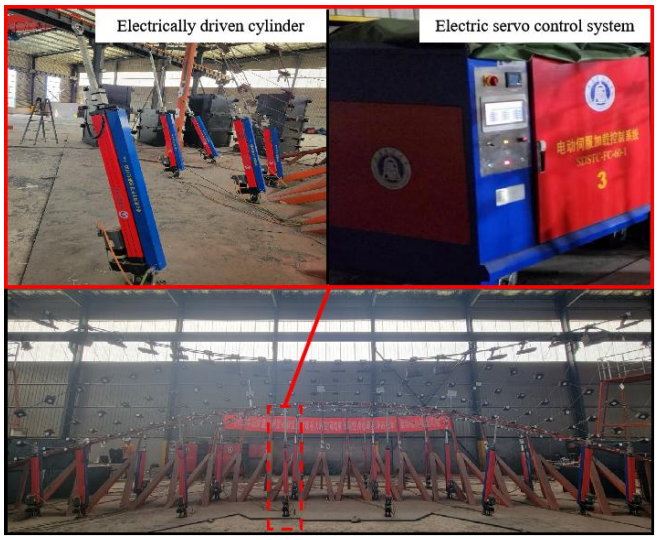

3.3. Measurement equipment and measurement point layout

In the cable force monitoring, S-type load cells and anchor cable force sensors were used. The Midas computational model for the actual engineering project provided the envelope values of internal and reaction forces. In the model test, these forces were scaled to 1/100 of the actual values. For the load-bearing cables, S-type tension and compression sensors with a 2 tons capacity were used, with 3 sensors in total. The anti-wind and edge cables were fitted with S-type tension sensors with a 10 tons capacity, totaling 10 sensors. The diagonal cables were monitored with anchor cable force sensors, each with a 50 tons capacity. During the loading process, a total station paired with laser reflectors was used to monitor structural deformation. The arrangement of the measurement equipment is shown in Fig 7.

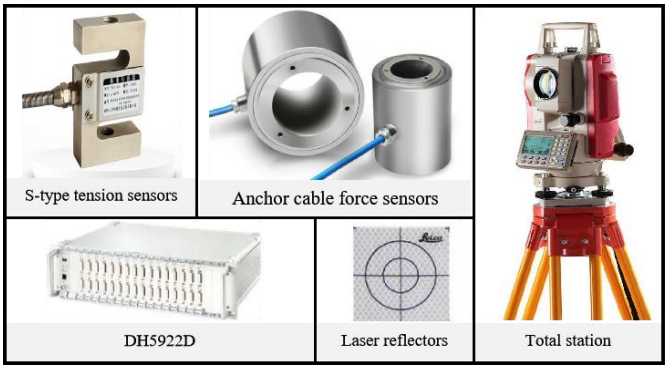

Fig. 7 Measuring equipments

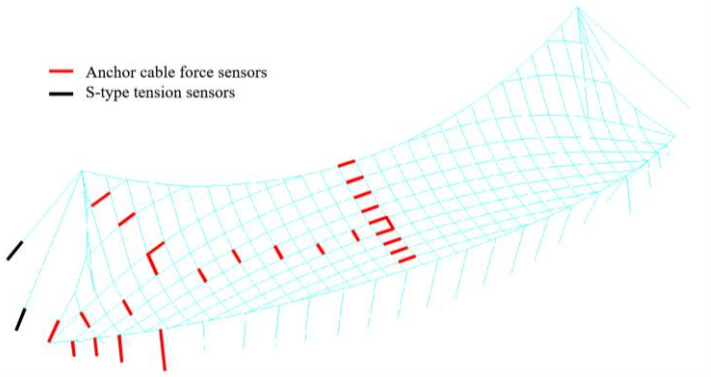

(a) Layout of cable force measurement points

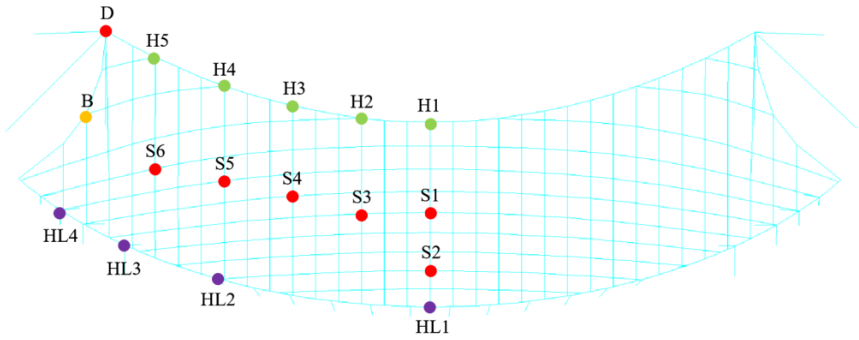

(b) Layout of deformation measurement points

Fig. 8 Layout of measurement points

This experiment included 28 cable force measurement points, as shown in Fig 8(a). A total of 36 displacement measurement points were also arranged. These included 2 at the mast tops, 2 at the edge cables, 4 at the bases of the diagonal cables, 9 on the annular cables, 10 on the cable net, 7 on the ring beam, and 2 at the bottom of the ring beam. The detailed arrangement is shown in Fig 8(b).

4. Test result

Under three loading conditions, the tensile forces and displacements of the single-layer cable net structure were measured. Loading case 1 includes dead load and live load, Loading case 2 includes dead load and wind pressure load, and Loading case 3 includes dead load and wind suction load. The loading levels range from 5, with each level increasing by 20%.

4.1. Case I

4.1.1. Changes in cable force

The variation in cable force at the measurement points under Case I is shown in Fig. 9. As the load increased linearly, the cable forces also exhibited a linear increase. During the incremental loading process, the tension in the HS cables reached its maximum, identifying them as the primary load-bearing components of the structure. The internal force in XS1 was approximately 6% greater than that in XS2, while the internal forces in the four BS cables showed relatively minor differences. Notably, the tension in the load-bearing cables varied with the loading level depending on their specific positions. Most of the tensions in the CS cables increased with the applied load; however, the tensions in CS0, CS4, and CS8 gradually decreased. The variations in the tensions of KS2, KS9, KS10, and KS11 were relatively small, whereas the tensions in the remaining KS cables progressively decreased, with KS9 maintaining a consistently higher tension level.

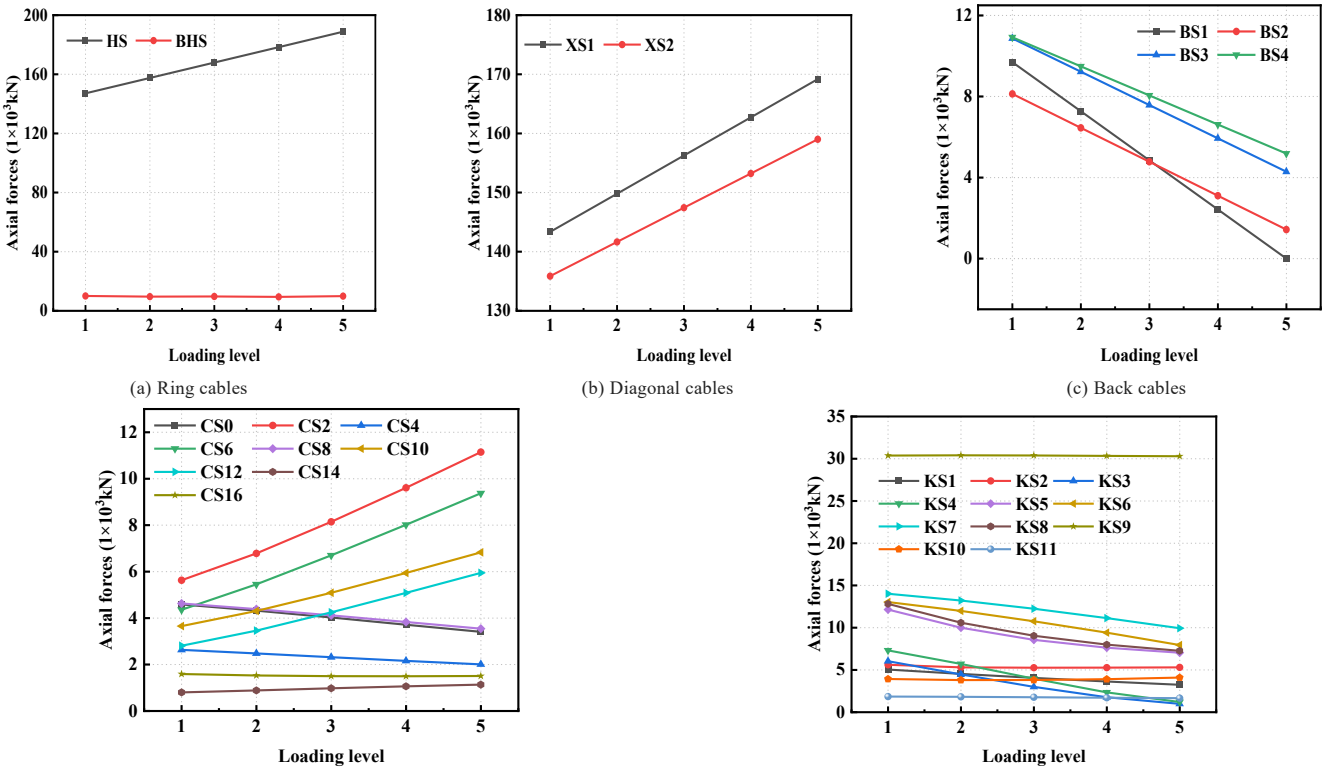

(a) Ring cables (b) Diagonal cables (c) Back cables

(d) Load-bearing cables (e) Anit-wind cables

Fig. 9 Changes in the cable force at the measurement point under Case I

4.1.2. Changes in displacement

The variation in displacement at the measurement points under Case I is shown in Fig. 10. As the load increased, the displacement of the cable net decreased approximately linearly. With the external load increasing from Level 1 to Level 5, the maximum vertical displacement of the structure occurred at measurement point S6 on the cable net, reaching 80 mm. The displacement at the ring beam node HL gradually increased, with a more pronounced upward trend observed at HL1, where the maximum displacement reached 9.95 mm. At the flexible boundary of the cable net, the displacement at measurement point B increased by approximately 13.78 mm, while the displacement at measurement point D, located at the top of the mast, exhibited relatively small variations.

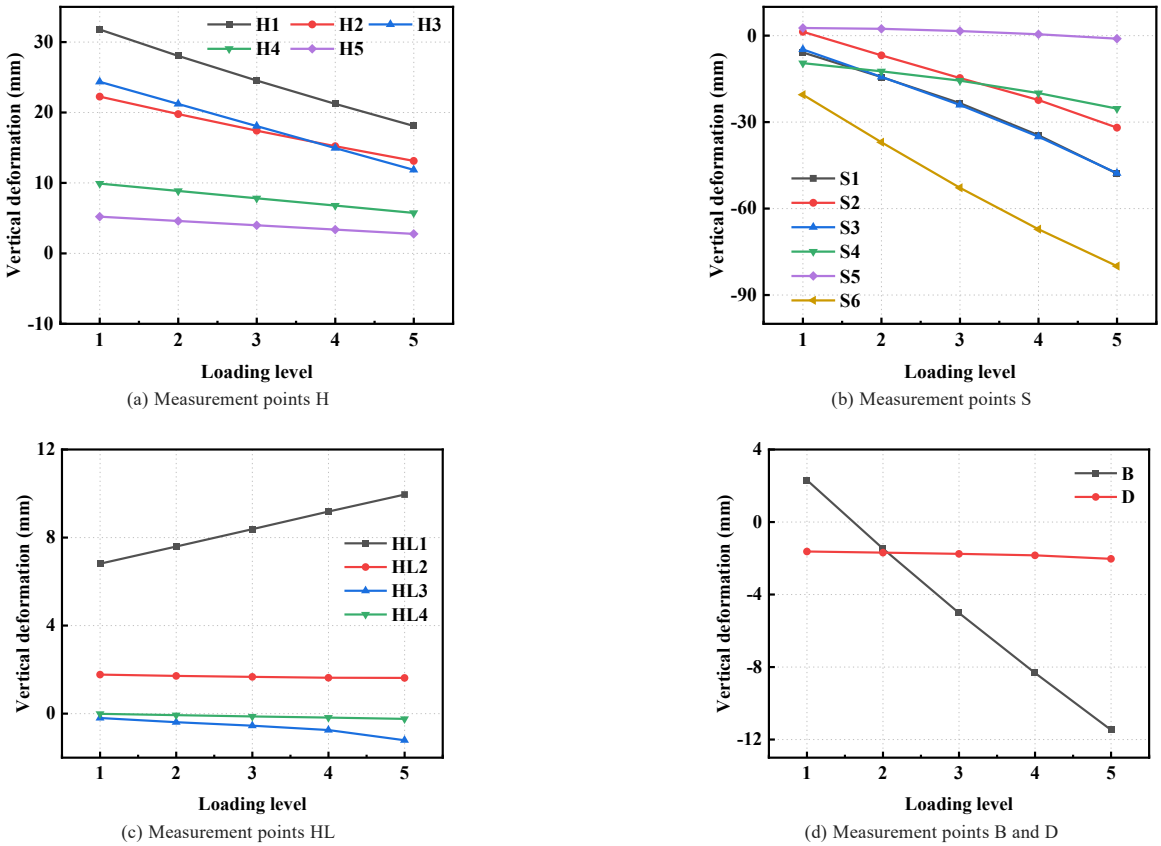

(a) Measurement points H

(b) Measurement points S

(c) Measurement points HL

(d) Measurement points B and D

Fig. 10 Changes in the displacement of the measuring point under Case I

4.2. Case II

4.2.1. Changes in cable force

The variation in cable force at the measurement points under Case II is shown in Fig. 11. As the load increased, the cable forces at the measurement points increased approximately linearly. The variation pattern closely resembles that observed in Case I, with the ring cables continuing to serve as the primary load-bearing components of the structure. The internal force in XS1 consistently exceeds that in XS2, and the differences in force among the four backstay cables remain relatively small. Notably, after the fourth loading level, BS1 and BS2 exhibit signs of force relaxation. While most of the forces in the CS cables increase with the applied load, the forces in CS0, CS4, and CS8 gradually decrease. The force variations in KS2, KS9, KS10, and KS11 are relatively minor, whereas the forces in the remaining KS cables gradually decline, with KS9 maintaining a comparatively higher force level.

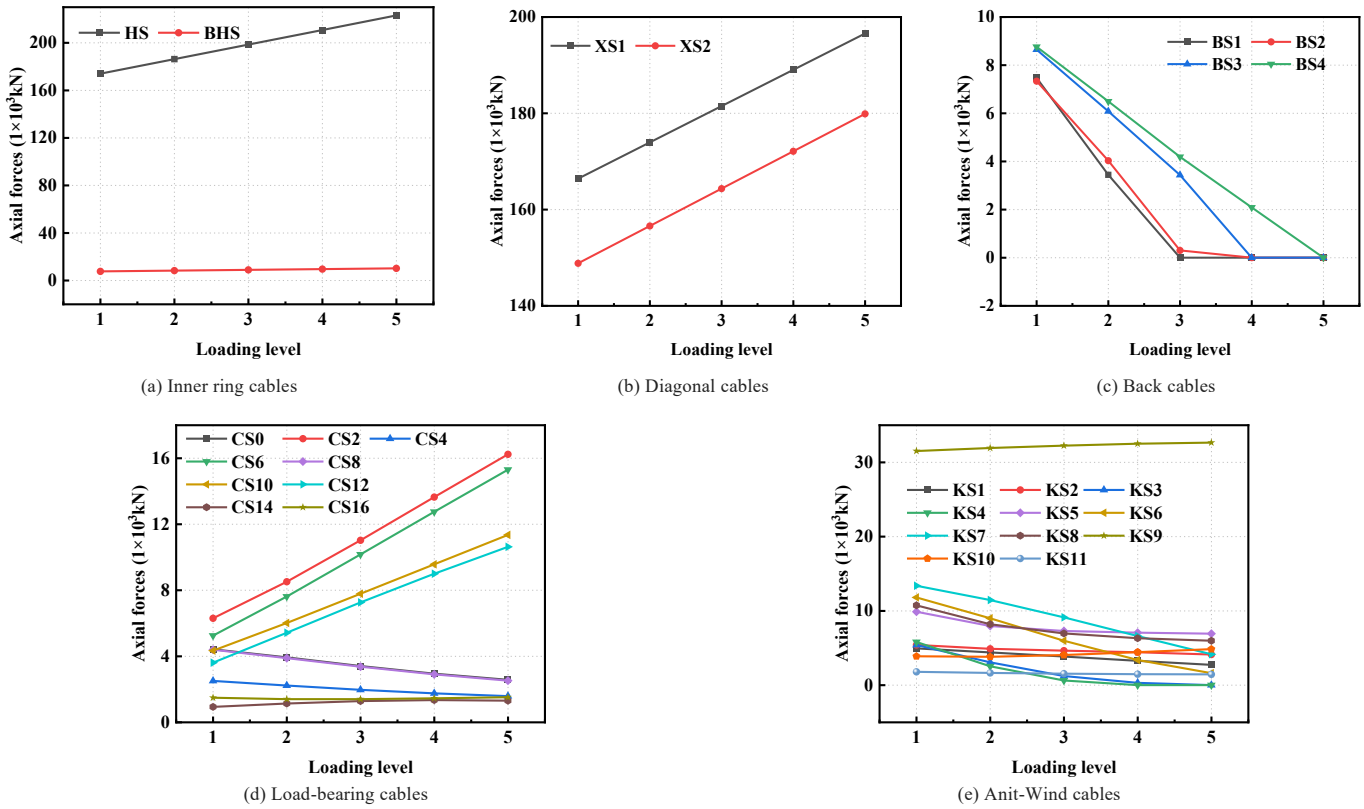

(a) Inner ring cables

(b) Diagonal cables

(c) Back cables

(d) Load-bearing cables

(e) Anit-Wind cables

Fig. 11 Changes in the cable force at the measurement point under Case I

4.2.2. Changes in displacement

The variation in displacement at the measurement points under Case II is shown in Fig. 12. As the load increased, the displacements at each measurement point decreased approximately linearly. The overall pattern of vertical displacement at the nodes is generally consistent with that observed in Case I, with the maximum vertical displacement still occurring at cable-net measurement point S6, reaching 129.6 mm. The displacement at ring cable measurement point H5 gradually increases, while the displacements at the remaining measurement points decrease. At the rigid boundary, the vertical displacement at measurement point HL1 exhibits a noticeable increasing trend, whereas the displacement variations at other rigid boundary points are relatively minor. At the flexible boundary, the displacement at measurement point B increases by approximately 22.23 mm, while the variation in displacement at the top of the mast (measurement point D) remains relatively small.

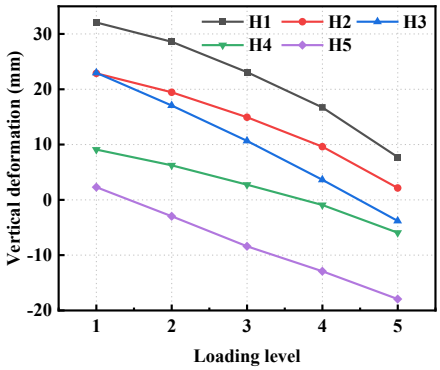

(a) Measurement points H

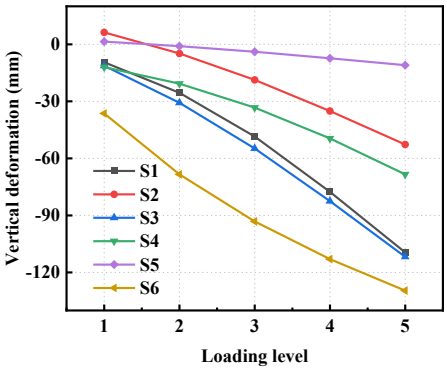

(b) Measurement points S

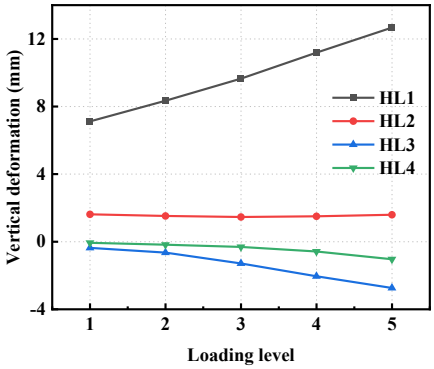

(c) Measurement points HL

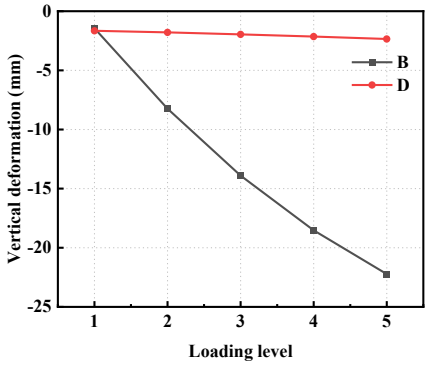

(d) Measurement points B and D

Fig. 12 Changes in the displacement of the measuring point under Case II

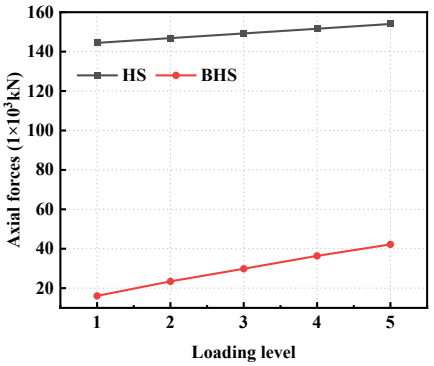

(a) Inner ring cables

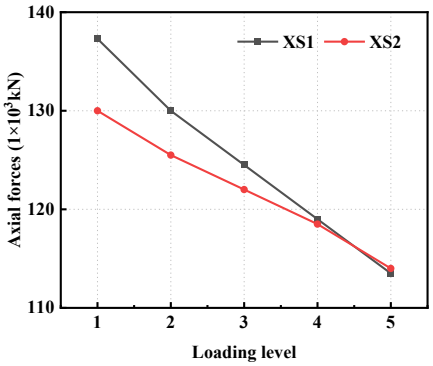

(b) Diagonal cables

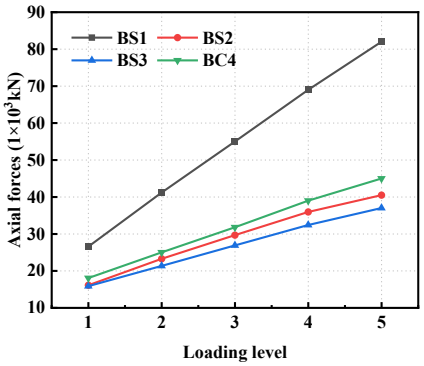

(c) Back cables

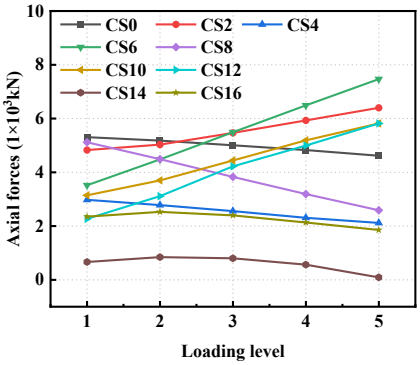

(d) Load-bearing cables

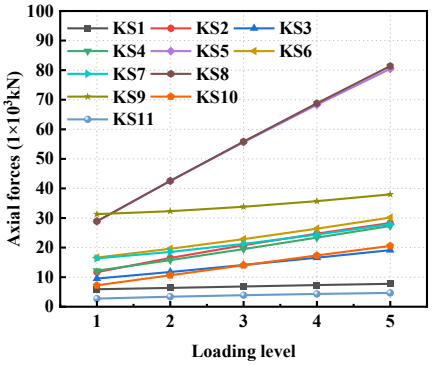

(e) Anit-wind cables

Fig. 13 Changes in the cable force at the measurement point under Case I

4.3 Case III

4.3.1. Changes in cable force

The variation in displacement at the measurement points under Case III is shown in Fig. 13. Unlike Cases I and II, Case III incorporates both dead load and wind suction load, representing a fundamentally different loading scenario. In addition to HS, the internal forces in the BHS components also exhibit a noticeable upward trend, with HS remaining the component subjected to the highest tensile force. In contrast to the previous two cases, the internal forces in the XS components decrease linearly, and by loading level 5, the tensile force in XS2 exceeds that in XS1. The tensile forces in all four BS components increase significantly, with BS1 showing the most pronounced growth. Among the CS components, the tensile forces in CS2, CS6, CS10, and CS12 increase with the load, while those in the remaining CS elements decrease to varying degrees. All KS components exhibit an increasing trend in tensile force, with KS5 and KS8 showing the most distinct patterns. Notably, the tensile forces in KS5 and KS8 are nearly identical throughout the loading process.

4.3.2. Changes in displacement

The displacement variation curves of the measurement points under Case III are presented in Fig. 14. As the load increases linearly, the vertical displacement at measurement point H on the ring cable also increases to varying degrees. The closer the point is to the mast, the smaller the magnitude of vertical displacement observed. The maximum displacement still occurs at mesh measurement point S6, reaching 194.8 mm. Displacements at the other S points also increase approximately linearly with the applied load. For the rigid ring beam, the displacement at measurement point HL1 decreases, while the displacements at the other HL points show a linear increase with loading. Similar to Cases I and II, the displacement at the mast top remains nearly unchanged. At the flexible boundary, measurement point B exhibits a clear linear displacement trend in the opposite direction.

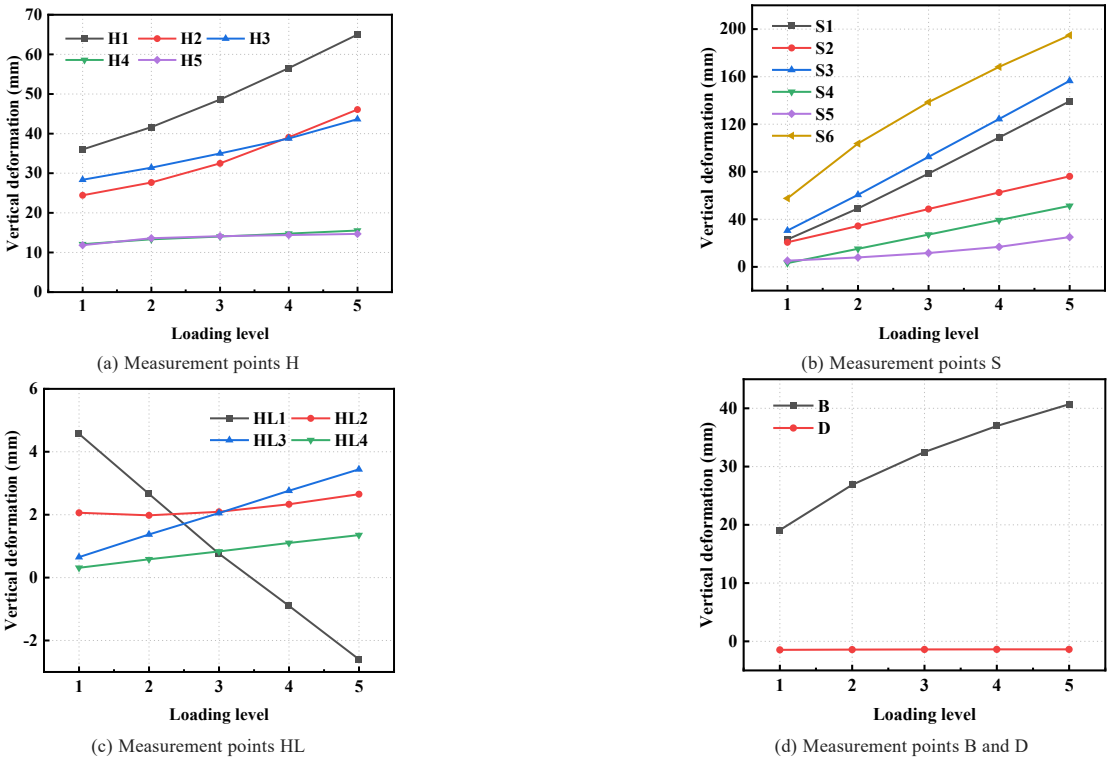

(a) Measurement points H

(b) Measurement points S

(c) Measurement points HL

(d) Measurement points B and D

Fig. 14 Changes in the displacement of the measuring point under Case III

5. Finite element analysis

5.1.Model details

For the experimental model of the single-layer cable net structure, a numerical model is established using the general-purpose finite element software ANSYS. This model includes the single-layer saddle-shaped cable net and the supporting steel structure. All cables are modeled using the LINK180 element, which can be configured via the KEYOPT switch to allow only tensile behavior. The cable mesh structure is prestressed by adding cell initial strains in order to apply prestress. The supporting steel structure, including steel masts, ring beams, and struts, is modeled using BEAM188 elements. The cable clamps are simulated using MASS21 elements[23]. The finite element model is shown in Fig. 15, with the material properties of the components listed in the Table 5.

Table 5
Material mechanics parameters in finite element model

Members	Elastic modulus E (MPa)	Thermal expansion coefficient α (1/℃)	Density ρ
Cables	1.9×10^5	1.2×10^{-5}	7.85×10^3
Steel members	2.06×10^5	1.2×10^{-5}	7.85×10^3

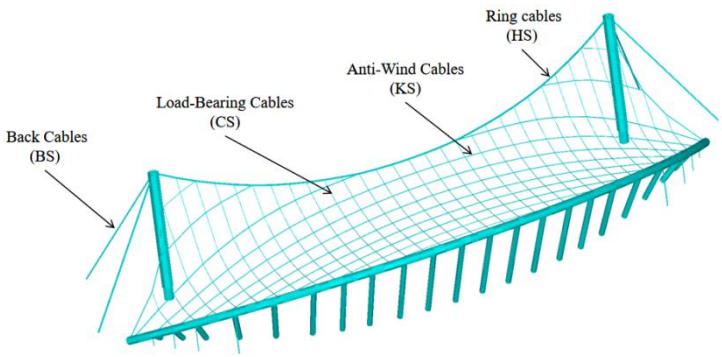

Fig. 15 Finite element model

5.2.FEM verification

5.2.1.Comparison of cable forces

The three types of load cases used in the experiment were successfully simulated, with both the loading method and loading points consistent with the experimental setup. Due to the large volume of data, Fig. 16 presents the comparison of cable forces between the experimental and finite element results for each cable under Load Case I. The measured displacements closely match the numerically calculated values, and the overall trends are in good agreement.

Fig. 17 shows the comparison of cable forces at each measurement point under Load Case I. The results indicate that the cable forces under different loading conditions exhibit similar trends in both the test and simulation, with only minor discrepancies. However, across Load Cases I, II, and III, the largest average deviation in cable force occurs at measurement point XS1, with average errors of 10.6%, 11.1%, and 10.5%, respectively. A detailed comparison of the internal cable forces at XS1 under the three loading conditions is provided in Table 6.

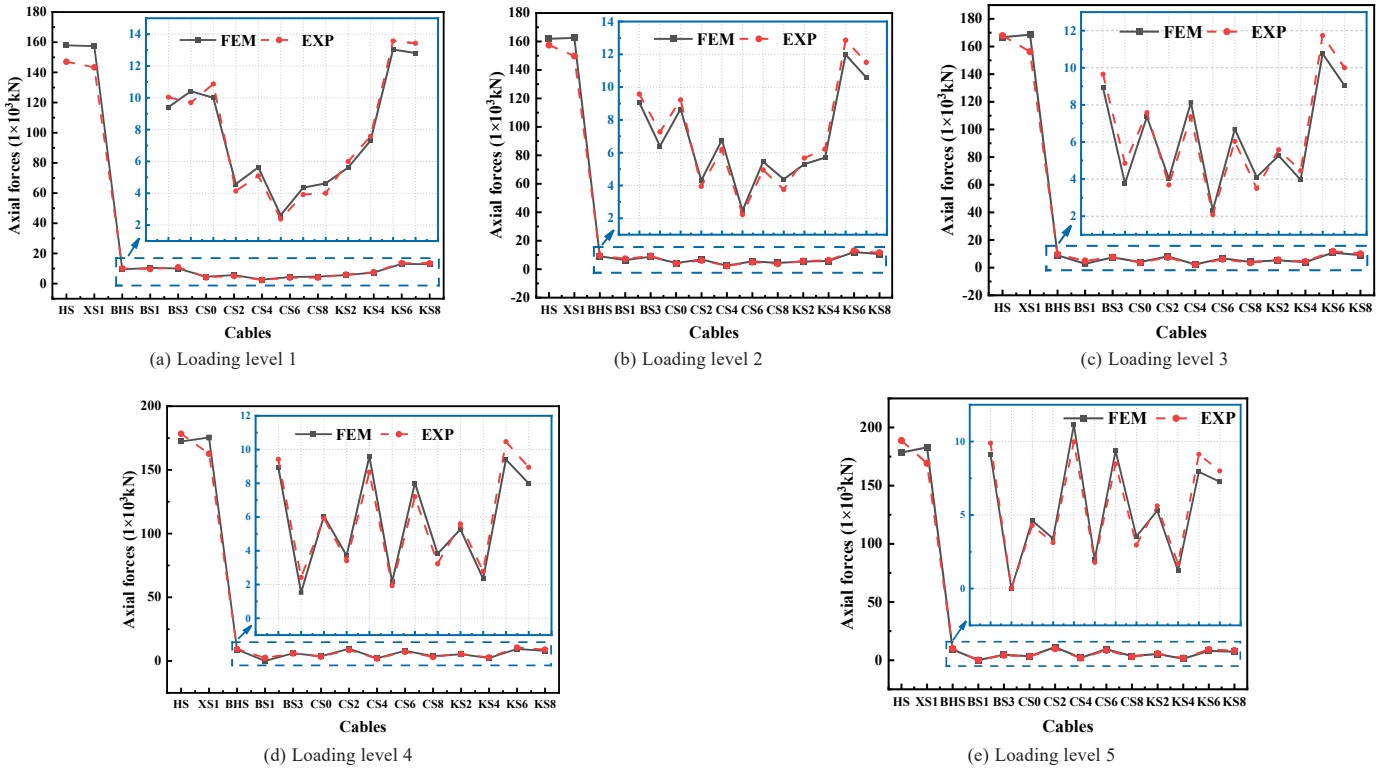

(a) Loading level 1 (b) Loading level 2 (c) Loading level 3

(d) Loading level 4 (e) Loading level 5

Fig. 16 Comparison of cable force

Table 6
Comparison of cable forces at measuring point XS 1

Loading cases	Loading levels	Cable force (kN) FEM	Cable force (kN) EXP	Deviation(%)
I	1	157.65	143.34	9.98
	2	165.37	149.80	10.40
	3	172.89	156.26	10.65
	4	180.42	162.71	10.88
	5	187.95	169.17	11.10
II	1	166.42	150.12	10.86
	2	173.96	155.73	11.71
	3	181.49	166.44	9.04
	4	189.03	169.55	11.49
	5	196.57	174.86	12.42
III	1	137.30	124.44	10.33
	2	130.11	118.56	9.74
	3	124.51	113.68	9.53
	4	119.22	106.81	11.62
	5	113.49	101.92	11.35

5.2.2. Comparison of displacement

Due to the large volume of data, Fig. 17 displays only the displacement comparison charts between the experimental and finite element results for each measurement point under Load Case I. The measured displacements exhibit good agreement with the simulation results, and the overall trend is consistent. However, under Load Cases I, II, and III, the largest average vertical displacement error occurs at measurement point S3, with deviations of 10.79%, 11.68%, and 11.29%, respectively. Table 6 presents a comparison of the internal forces of cable S3 across the three loading cases.

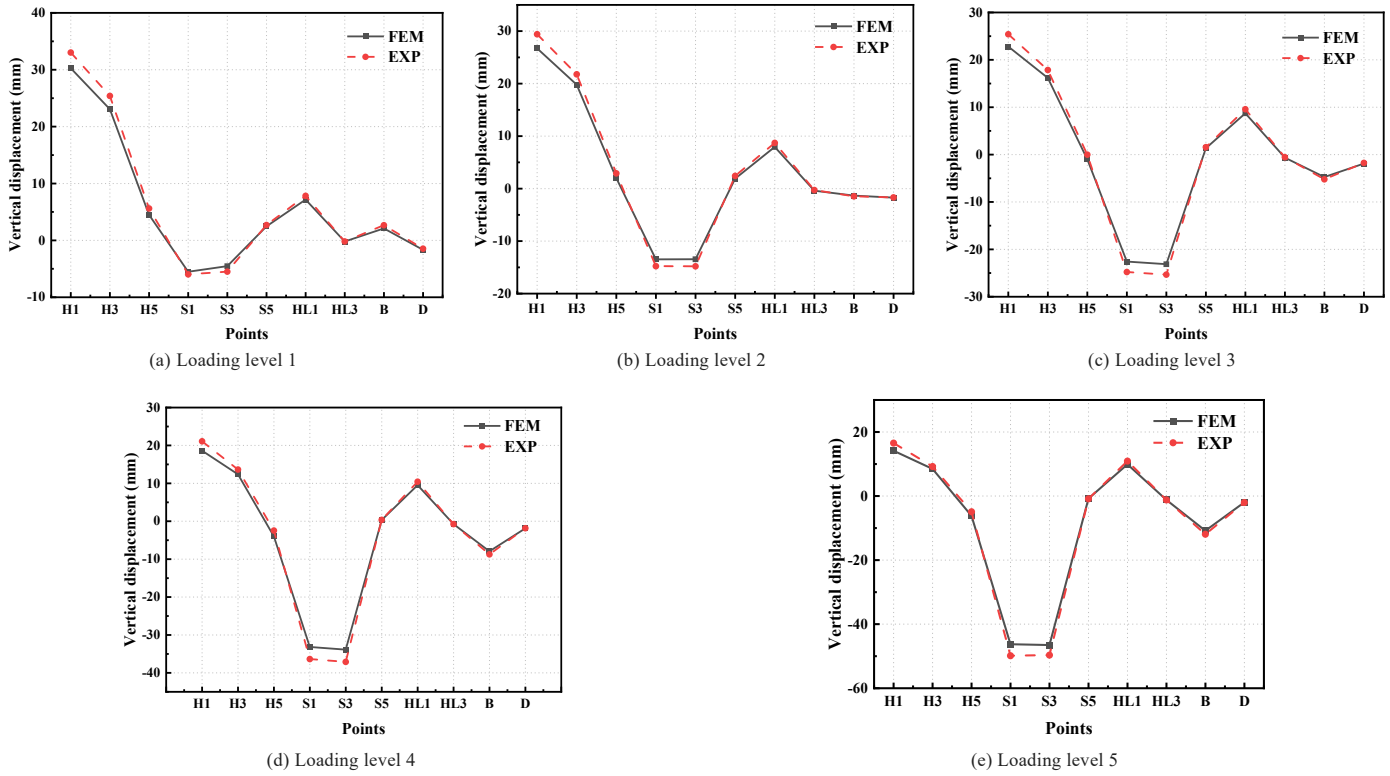

(a) Loading level 1 (b) Loading level 2 (c) Loading level 3

(d) Loading level 4 (e) Loading level 5

Fig. 17 displacement comparison chart

Table 7
Displacement comparison of measuring point S3

Loading cases	Loading levels	displacement (mm) EXP	displacement (mm) FEM	Deviation (%)
I	1	-4.44	-4.93	11.04%
	2	-13.26	-14.8	11.61%
	3	-23.04	-25.35	10.03%
	4	-33.88	-37.11	9.52%
	5	-44.45	-49.68	11.77%
II	1	-12.89	-11.3	-12.32%
	2	-33.35	-30.75	-10.48%
	3	-61.40	-54.8	-10.75%
	4	-93.35	-82.5	-11.62%
	5	-128.83	-111.8	-13.22%
III	1	31.32	34.91	11.46%
	2	62.29	69.07	10.00%
	3	95.38	105.94	11.05%
	4	125.25	141.08	12.64%
	5	159.49	177.54	11.32%

6. Conclusions

In this study, the roof structure of the Xiatian Cultural Park Stadium was selected as the research subject. A static load test was conducted on a 1:10 scaled physical model to investigate the performance of a novel single-layer saddle-shaped cable network system. The structural behavior under various loading conditions was analyzed through both experimental testing and finite element simulation. The main conclusions are as follows:

(1) In the static loading tests of flexible cable-net structures, the electro-servo loading control system effectively regulates both the load application rate and load ratios. This ensures that the test results accurately capture the response characteristics of the prototype structure under static loading, thereby meeting the required accuracy standards. Moreover, this approach provides valuable reference data for subsequent model tests of similar structural systems.

(2) During the progressive application of static loads, the forces in each cable group and the nodal displacements exhibit linear variations corresponding to the load increments. The finite element analysis results demonstrate a high degree of correlation with the experimental data in terms of overall trends, with discrepancies maintained within acceptable limits. This strong agreement validates the accuracy of the numerical simulation approach and confirms the reliability of the experimental procedures, thereby providing a robust reference for structural engineering applications.

(3) The reduction in forces observed in some load-bearing cables is attributed to the arrangement of the load attachment points. Due to spatial constraints imposed by the loading equipment beneath the cable net, the uniformly distributed load attachment points were limited to 22. This limitation caused localized high tension within the cable net and corresponding reductions in tension in adjacent areas, resulting in force loss in certain load-bearing cables. Therefore, future experiments of this nature should focus on further optimizing the layout of load attachment points to improve their distribution and rationality.

Acknowledgments

This research was funded by Hebei Natural Science Foundation, grant

number E2024508238 and Hebei Key Laboratory of Civil Engineering Catastrophe Control and Disaster Emergency Response, grant number HBHK2024-1.

References

[1] Vaezzadeh A, Ahmadizadeh M, Dolatshahi KM. Three-dimensional nonlinear dynamic analysis of slack cable structures using node Relaxation method[J]. Structures, 2021, 29: 586-599.
[2] Cinquini C, Contro R. Prestressing design method for cable net structures[J]. Engineering Structures, 1985, 7: 183-189.
[3] Yan P F, Liu C L, Liu B D, et al. Static Load Test of Cable Net Structure of Xi'an International Football Center with Scaled Model[J]. Progress in Steel Building Structures, 2024, 26(10), 74-87.
[4] Zhang D, Liu TQ, Li S, et al. Three-dimensional laser scanning for large-scale as-built surveying of 2022 Beijing Winter Olympic Speed Skating Stadium: A case study[J]. Journal of Building Engineering, 2022, 59: 105075.
[5] Schek H-J. The force density method for form finding and computation of general networks[J]. Comput Methods Applied Mechanics and Engineering, 1974, 3: 115-134.
[6] Li X, Liu C, Xue S, Li X, Zhang C, Huang L, et al. The modified force density method for form-finding of cable net structure[J]. Thin-Walled Structures, 2024, 195: 111363.
[7] Li X, Xue S, Liu Y. A novel form finding method for minimum surface of cable net[J]. Journal of Building Engineering, 2022, 48: 103939.
[8] Lv H, Jiaming Z, Zhongyi Z, et al. Study on prestress distribution and structural performance of heptagonal six-five-strut alternated cable dome with inner hole[J]. Structures, 2024, 65: 106724.
[9] Huiyun W. Construction Methods for the Calgary Saddleback Stadium - Indoor Stadium for the 1988 Winter Olympics[J]. Building Construction, 1984, 05: 75-76.
[10] Ma S, Chen M H, Dong Y C, et al. Statics and dynamics of pulley-driven tensegrity structures with sliding cable modeling[J]. Applied Mathematical Modelling, 2024, 130, 378-400.
[11] Shichang Z, Xiaoming X, Feng G. Structural design of the steel roof of the swimming pool of Suzhou Olympic Sports Center[J]. Building Structure, 2019, 49, (23).
[12] Shudong G, Jingxun Z, Cunzhi Z, et al. Research on the overall installation program of the large-span saddle-shaped cable network structure of the National Speed Skating Pavilion[J]. Building Technology, 2020, 50(03): 333-336.
[13] Ningyuan Z, Bin L, Lei Z, et al. Research on the forming technology of a novel type structure of double-layer orthogonal cable net with a large opening[J]. Structures, 2024, 63: 106371.
[14] Mingliang Z, Jin W, Jiaming G. Physics-informed radial basis networks for force finding of cable domes[J]. Thin-Walled Structures, 2025, 206: 112675.
[15] Yaqiong T, Qing Lv, Tuanjie L, et al. Self-equilibrium, stability, and accuracy degradation of imperfect prismatic tensegrities with additional cable nets[J]. Engineering Structures, 2023, 284, 115981.
[16] F Benedettini, Rega G. Planar non-linear oscillations of elastic cables under superharmonic resonance conditions[J]. Journal of Sound and Vibration, 1989, 132(3): 353-366.
[17] Lu Yang, Shi Ga ng, Yin Hao, et al. Full-scale experimental study on the influence of damages on the static behavior of the single-layer cable net structure[J]. Structures, 2015, 3153-162.
[18] Fabio Rizzo, Caracoglia Luca. Examination of artificial neural networks to predict windinduced displacements of cable net roofs[J]. Engineering Structures, 2021, 245112956.
[19] Sun F, Y-Q W, Y-J S, et al. The inflection performance analysis of the complex single layer cable net under horizontal load[J]. Oxford: Elsevier Science Ltd, 2005: 395-399.
[20] Guojun S, Shuo X, Jinzhi W. Study on mechanical properties of truss cable structure under low cyclic loading[J]. Journal of Building Engineering, 2022 , 58: 105051
[21] Guojun S, Shuo X, Jinzhi W, et al. Shaking table test and simulation on seismic performance of aluminum alloy reticulated shell structures under elastic and elastic-plastic stage[J]. Journal of Building Engineering, 2024, 110878.
[22] Load Code for Building Structures[S], Beijing, China Construction Industry Press,2012.
[23] Amin V, Kiarash M D. Progressive collapse resistance of cable net structures[J]. Journal of Constructional Steel Research, 2022, 195:107347.